J Mater Sci (2008) 43:503–509
DOI 10.1007/s10853-007-1822-4

5TH BRAZILIAN MRS MEETING

Ac and dc magnetotransport properties of the phase-separated $La_{0.6}Y_{0.1}Ca_{0.3}MnO_3$ manganite

F. C. Fonseca · J. A. Souza · E. N. S. Muccillo · R. Muccillo · R. F. Jardim

Received: 20 December 2006 / Accepted: 4 May 2007 / Published online: 20 July 2007

Abstract The physical properties of the $La_{0.6}Y_{0.1}Ca_{0.3}MnO_3$ compound have been investigated, focusing on the magnetoresistance phenomenon studied by both dc and ac electrical transport measurements. X-ray diffraction and scanning electron microscopy analysis of ceramic samples prepared by the sol–gel method revealed that specimens are single phase and have average grain size of ~0.5 μm. Magnetization and 4-probe dc electrical resistivity $\rho(T,H)$ experiments showed that a ferromagnetic transition at $T_C \sim 170$ K is closely related to a metal-insulator (MI) transition occurring at essentially the same temperature T_{MI}. The magnetoresistance effect was found to be more pronounced at low applied fields ($H \leq 2.5$ T) and temperatures close to the MI transition. The ac electrical transport was investigated by impedance spectroscopy $Z(f,T,H)$ under applied magnetic field H up to 1 T. The $Z(f,T,H)$ data exhibited two well-defined relaxation processes that exhibit different behaviors depending on the temperature and applied magnetic field. Pronounced effects were observed close to T_C and were associated with the coexistence of clusters with different electronic and magnetic properties. In addition, the appreciable decrease of the electrical permittivity $\varepsilon'(T,H)$ is consistent with changes in the concentration of e_g mobile holes, a feature much more pronounced close to T_C.

F. C. Fonseca (✉) · E. N. S. Muccillo · R. Muccillo
Instituto de Pesquisas Energéticas e Nucleares, CP 11049, São Paulo, SP 05422-970, Brazil
e-mail: cfonseca@ipen.br

J. A. Souza · R. F. Jardim
Departamento de Física dos Materiais e Mecânica, Instituto de Física, Universidade de São Paulo, CP 66318, São Paulo, SP 05315-970, Brazil

Introduction

Mixed-valence manganites with the $RMnO_3$ perovskite structure have attracted a great deal of interest due to their intriguing properties such as metal-insulator transition (MI) and colossal magnetoresistance (CMR) [1]. These phenomena arise from the intrinsically inhomogeneous states of CMR manganites and the strong interplay between magnetic, electronic, and structural degrees of freedom [2, 3]. In these perovskites, the competition between different ordering tendencies leads to changes in their properties upon the application of relatively small perturbations [2]. Recent studies have indicated that the properties of these materials are related to intrinsic inhomogeneities due to disorder caused by the chemical-doping process [4–6]. Such an intrinsic disorder would induce spatially separated phases with different electronic and magnetic properties appearing far above the ferromagnetic transition temperature T_C [4]. The level of disorder is the key variable defining the length scale of each phase and the metal-insulator transition is treated in a percolative framework where the conduction through metallic or insulating phases alternatively dominates the transport properties below and above the metal-insulating transition temperature, T_{MI}, respectively. Magnetoresistive properties in these systems are also explained as the result of altering the initial equilibrium between phases, the applied magnetic field favoring and enlarging the FM and metallic domains at the expense of the insulating ones [4].

Therefore, the understanding of the transport properties of manganites has been associated with two important mechanisms. The first one is termed intergranular magnetoresistance (IMR), and its signature is a large drop of the electrical resistivity at relatively low applied magnetic fields in polycrystalline samples, a feature absent in

single-crystal specimens [7, 8]. The second one is the phase separation (PS) scenario, in which a magnetic separation of phases with different spin dynamics has been theoretically predicted and experimentally observed [3, 6, 9]. The emerging CMR picture is based on nanoscale clusters of competing phases, and at present, the existence of mixed-phase in the CMR regime is widely accepted [2, 6]. With increasing magnetic field, the ferromagnetic (FM) clusters with metallic characteristics rapidly align their moments, leading to a percolative insulator-metal (MI) transition [3]. Thus, the CMR effect is understood as the competition between the FM and insulator antiferromagnetic (AFI) and paramagnetic (PM) phases controlled by both temperature and applied magnetic field.

The physical properties of these manganites are very sensitive to the relative concentration of Mn^{3+} and Mn^{4+} in the octahedral sites, and the proportion of these two cations is usually changed by a partial substitution of the trivalent R ion by divalent cations, i.e., adding mobile e_g carriers to the system. Within this context, the $La_{1-x}Ca_xMnO_3$ phase diagram has been previously reported [10]. In the x range $0.2 \leq x \leq 0.5$, these compounds exhibit both FM ordering and metallic conductivity owing to the double exchange DE interaction between Mn^{3+}–Mn^{4+} pairs. On the other hand, the influence of La^{3+} substitution by Y^{3+} on $La_{1-x}Ca_xMnO_3$ has already been reported [11, 12]. The main effect of such a substitution is the local modification of the Mn–O–Mn bond angle due to the smaller ionic radius of Y^{3+}, resulting in an increased disorder [4]. The distortion of this bond angle disrupts the long range order of the FM of the pristine compound $La_{0.7}Ca_{0.3}MnO_3$, which occurs at $T_C \sim 250$ K, and changes the carrier mobility increasing the electrical resistivity, with little effect on the carrier (hole) concentration. A decrease of the FM and metal-insulator MI transition temperatures, T_C and T_{MI}, respectively, with increasing Y^{3+} is also observed and the colossal magnetoresistance CMR effect is largely enhanced, a feature probably related to the increased spin frustration with increasing Y^{3+} concentration. In addition, this chemical substitution gives rise to a clustered state well above T_C, where metallic and insulating phases coexist in a wide temperature range [4].

The ac transport of the phase-separated manganites has already been studied [13–17]. The reported results revealed that the electrical conductivity and the CMR effect are frequency dependent and indicated the percolative nature of the MI transition. In addition to this, impedance spectroscopy $Z(f,T)$ measurements revealed two relaxation processes in the frequency domain [18–20]. The $Z(f,T)$ is widely used for electrical characterization of materials and is a powerful technique for separating contributions to the electrical resistivity due to grains (bulk) and to internal surfaces such as grain boundaries and extra phases [21, 22]. The analysis of the $Z(f,T)$ measurements in manganites indicated that the observed relaxation processes are related to the coexistence of clusters with different spins dynamics, essentially FM and AFI/PM phases [18, 19].

In this paper, we describe the results of a systematic investigation on the magnetotransport properties of high-quality $La_{0.6}Y_{0.1}Ca_{0.3}MnO_3$ samples prepared by the sol–gel technique. The combined results of both dc and ac magnetoresistivity of Y substituted $La_{0.7}Ca_{0.3}MnO_3$ compound indicated that frequency-dependent transport experiments, such as impedance spectroscopy, under applied magnetic field can be useful for investigating the transport properties of these phase separated manganites.

Experimental

Polycrystalline samples of $La_{0.6}Y_{0.1}Ca_{0.3}MnO_3$ were prepared by the sol–gel method. Further details of the preparation method are described elsewhere [4, 23]. The phase characterization of ground specimens was performed by X-ray diffraction (XRD) analysis at room temperature using Cu Kα radiation in the 2θ range 20–80°, with 0.02° (2θ) step size, and 10 s counting time. The samples prepared by the sol–gel method were found to be single phase, as revealed in the XRD pattern. The XRD data (not shown) were refined using the Rietveld method and all the observed diffraction peaks were indexed as belonging to the $La_{0.6}Y_{0.1}Ca_{0.3}MnO_3$ compound, space group *Pnma* [19]. The refined cell parameters are a = 5.4502 (5) Å, b = 7.6917 (3) Å, and c = 5.4511 (4) Å, in agreement with previously reported values [24].

The microstructure of the fractured surfaces of the ceramics samples was observed in a scanning electron microscope (SEM). The analyses of representative SEM images (not shown) indicate that the samples have a homogenous grain size distribution and are comprised of grains with average size $d_g \sim 0.5$ μm [19, 20]. The magnetic properties were studied by dc magnetization $M(T)$ measurements in the 5–300 K temperature range with applied magnetic field $H = 1$ kOe in both the zero-field cooled (ZFC) and field-cooled (FC) modes using a SQUID magnetometer. The dc electrical resistivity $\rho(T,H)$ was measured by the 4-probe technique using a LR-700 resistance bridge in applied magnetic fields H up to 5 T in the temperature range 5–300 K. The $\rho(T,H)$ measurements were performed by using both the magnetic field and temperature controls of the SQUID magnetometer. The impedance spectroscopy $Z(f,T,H)$ measurements were taken during warming from 77 K up to the room temperature using an Agilent 4294 impedance analyzer in the frequency (f) range 100 Hz–30 MHz with applied signal amplitude 20 mV and H up to 1 T. To vary the temperature

during the ac measurements, a quartz dewar filled with liquid nitrogen was used to insert a copper sample holder, the temperature was raised continuously, and monitored by a cernox thermometer. The dewar was placed between the poles of a water-cooled electromagnet which can generate magnetic fields up to ~1 T, as inferred from a calibrated Hall sensor. All transport measurements were performed using Ag paste contact pads and Cu leads.

Results and discussion

The combined results of both XRD and SEM analysis suggested that the samples prepared by the sol–gel method were single-phase and have a homogenous microstructure [19, 20]. Thus, let us now concentrate on the electrical and magnetic properties of the studied compound. The temperature dependence of the magnetic susceptibility $\chi(T)$, taken in ZFC and FC modes, are shown on the left inset of Fig. 1. The $\chi(T)$ curves exhibit a paramagnetic *PM* to ferromagnetic *FM* phase transition occurring at $T_C \sim 170$ K, defined here as the inflection point in the $\chi(T)$ curve. The $\chi(T)$ data were found to be essentially temperature independent below 100 K and no significant thermal irreversibility between the ZFC and FC curves has been observed.

The magnetic features observed have their counterpart in the dc electrical resistivity curves shown in Fig. 1. The

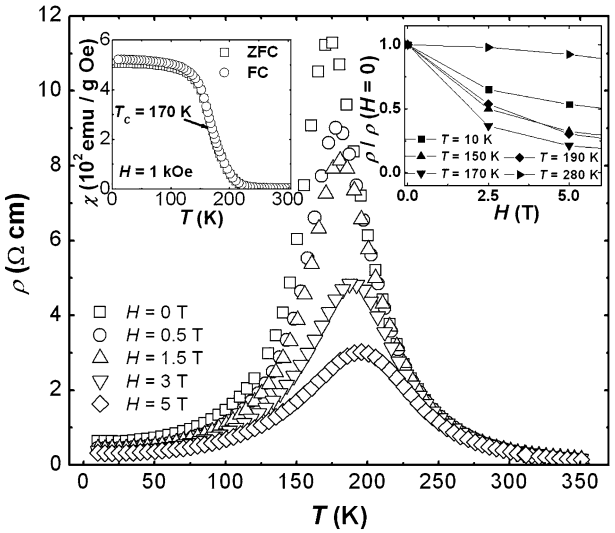

Fig. 1 Temperature dependence of the electrical resistivity of the $La_{0.6}Y_{0.1}Ca_{0.3}MnO_3$ compound measured under applied magnetic fields $H = 0$, 0.5, 1.5, 3, and 5 T. The right inset displays the ratio $\rho(H)/\rho(H = 0)$ as a function of the applied magnetic field at several temperatures $T = 10$, 150, 170, 190, and 280 K. The left inset shows the magnetization dependence on the temperature, measured in field cooled (FC) and zero-field cooled (ZFC) modes under an applied magnetic field of 1 kOe

temperature dependence of the $\rho(T,H = 0)$, reveals a MI transition at $T_{MI} \sim 175$ K, a temperature closely related to the *FM* transition (see left inset in Fig. 1). Increasing H results in the CMR effect, defined as a pronounced decrease of the $\rho(T)$ with H. In addition to this, T_{MI} is found to increase with increasing H, and reaches values close to $T_{MI} \sim 195$ K for $H = 5$ T. A large decrease (~70%) of the $\rho(T)$ is also observed for H up to ~2.5 T (see right inset of Fig. 1), which is associated with the negative CMR at low fields and frequently referred to intergranular magnetoresistance (IMR) [7]. Increasing H results in a further decrease of $\rho(T)$, however, for fields $H > 2.5$ T the $\rho(T,H)$ is significantly less magnetic field dependent. These features are observed at temperatures up to $T_{MI} \sim 175$ K, where the most pronounceable CMR effect (~80%) is reached at $H = 5$ T. At higher temperatures ($T \gg T_{MI}$), the decrease in $\rho(T)$ with H is less significant and has been attributed to the suppression of spin fluctuations [7].

The ac electrical properties of the $La_{0.6}Y_{0.1}Ca_{0.3}MnO_3$ compound were also investigated by impedance spectroscopy measurements $Z(f,T,H)$, as shown in Fig. 2(a) and (b). Typical impedance data measured at different temperatures and for both $H = 0$ and 1 T are shown in the Fig. 2. The $Z(f,T,H)$ data reveal two well-defined relaxation processes occurring at different frequency ranges: a high frequency (HF) one and another at lower frequencies (LF) [18, 19]. At high frequencies ($f > 10^7$ Hz), the HF component exhibits a parasite inductive (L) contribution, a feature related to the experimental set up. However, the L contribution has been estimated by using an equivalent circuit model, which was used for modeling the experimental diagrams. Such an equivalent circuit is constructed by the series association of two parallel resistor and capacitor elements, connected in series with the parasite L contribution [19]. The estimated value of $L \sim 2.5 \times 10^{-6}$ H was found to be temperature independent and the parasite contribution has been subtracted from the $Z(f,T,H)$ data. In addition, $Z(f,T)$ measurements with different applied amplitudes were carried out in order to assure that the two observed relaxations are due to the materials properties. These results (not shown) revealed that both HF and LF semicircles have an ohmic behavior and no appreciable changes of both components were observed in a large range of applied voltages. In addition, $Z(f,T,H)$ data of different samples have been measured indicating a good reproducibility of the experimental results. These combined experimental results indicate that both semicircles displayed in the $Z(f,T,H)$ data are indeed related to material properties and that at least two different transport processes take place in the frequency and temperature ranges studied.

Using the equivalent circuit model, the electrical resistance (R), capacitance (C), and the relaxation frequency $f_0 = (2\pi RC)^{-1}$ associated with both the HF and the LF

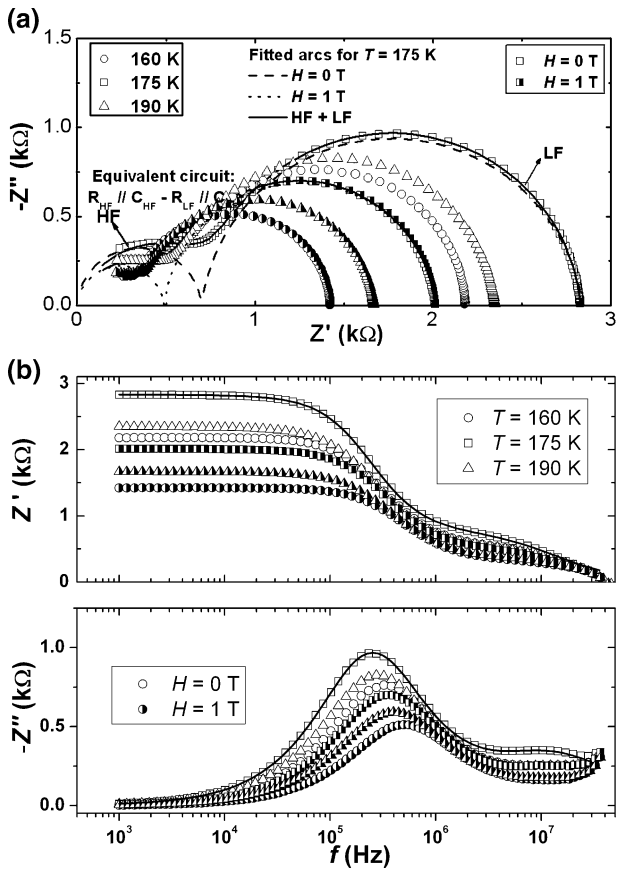

Fig. 2 Impedance spectroscopy data of the $La_{0.6}Y_{0.1}Ca_{0.3}MnO_3$ measured at $T = 160$, 175, and 190 K for $H = 0$ (open symbols) and 1 T (half-full symbols). The fitted HF and LF semicircles for $T = 175$ K are also presented. Both the complex plane diagrams (**a**) and the frequency dependence of the real and the imaginary parts of the impedance (**b**) are shown

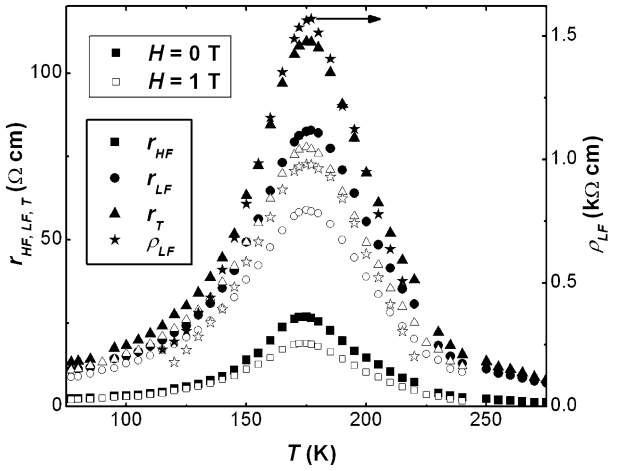

Fig. 3 Temperature dependence of the electrical resistivity determined after the $Z(f,T)$ diagrams of the $La_{0.6}Y_{0.1}Ca_{0.3}MnO_3$ sample for $H = 0$ and 1 T. r_{HF} corresponds to the electrical resistivity related to the high frequency component, r_{LF} to the low frequency one, r_T is defined as $r_{HF} + r_{LF}$, and ρ_{LF} is the specific resistivity of the low frequency component

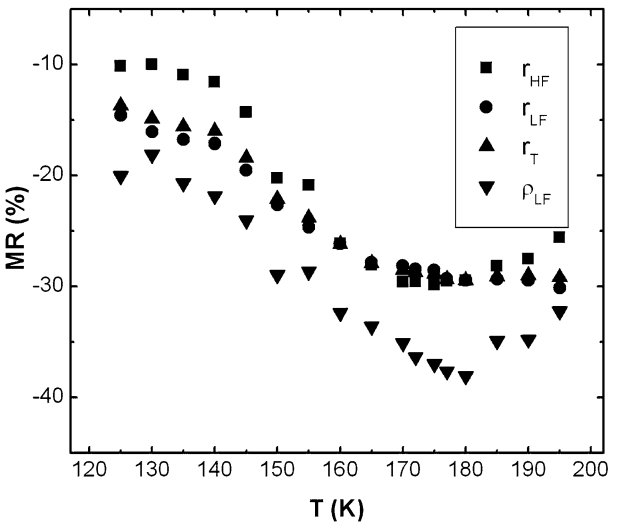

Fig. 4 Temperature dependence of the percent magnetoresistance MR(%) for the HF, LF, total, and specific resistivity components

semicircles were computed. The electrical resistivity associated with both the HF (r_{HF}) and LF (r_{LF}) components $r_{HF,LF} = k\ R_{HF,LF}$ was calculated using the geometrical factor $k = S/l$ (where S is the cross section area of the sample and l is the distance between voltage leads); the total electrical resistivity r_T is defined as the sum $r_{HF} + r_{LF}$. The temperature dependence of the HF, LF, and total components of the electrical resistivity for $H = 0$ e 1 T are shown in Fig. 3. These components display a MI transition at $T_{MI} \sim 175$ K for $H = 0$ T, a feature similar to the corresponding dc data displayed in Fig. 1. For $H = 1$ T, both the r_{HF} and the r_{LF} components decrease appreciably. The temperature dependence of the percent magnetoresistance, defined here as $MR(\%) = 100[(r(H = 1T) - r(H = 0))/r(H = 0)]$, for the different components is shown in Fig. 4. For temperatures below the MI transition, $T < T_{MI}$, the negative magnetoresistance is mainly governed by the decrease of the r_{LF} component (~15%) with applied H. The CMR effect related to the HF component exhibits a less pronounced contribution (~10%). The magnitude of the applied H used in the $Z(f,T,H)$ experiments is within the range where appreciable intergranular magnetoresistance (IMR) is usually seen $H < 2.5$ T, as observed in the dc data of Fig. 1 [7]. This result is relevant for the discussion involving CMR effects in manganites and indicates that: (a) the measured MR(%) at $H = 1$ T can be related to the rotation of magnetic domains (or clusters) and to finite size effects due to an increase of the FM cluster size; and (2) such an effect is mainly governed by the relaxation process which exhibits a more pronounced MR(%), i.e., that occurring at low frequencies (LF). In fact, the LF relaxation process observed in $Z(f,T)$ measurements is usually ascribed

to transport processes taking place at the internal surfaces of the material, such as the intergrain ones [21, 22], suggesting that the observed MR(%) can also be related to the IMR effect. Increasing the temperature from 120 K results in a maximum value of MR(%) ~ 30% close to T_{MI}. Further increase in T results in a decrease of MR(%) and, for $T \geq T_{MI}$, contributions to the magnetoresistance and related to both HF and LF components are indiscernible.

In addition to the electrical resistivity, the capacitive components associated with both the HF and LF relaxations were calculated. The obtained values were found to be weakly temperature dependent, and at temperatures close to T_{MI} they are $C_{HF} \sim 7.0 \times 10^{-13}$ F/cm and $C_{LF} \sim 1.2 \times 10^{-11}$ F/cm. In fact, the $C_{HF,\ LF}$ values are within the range for the capacitance associated with bulk and grain boundary (or an interface layer) contributions, respectively [25]. However, the experimental results reveal that a direct correspondence between the electrical resistance components (HF and LF) and the FM and AFI/PM phases is difficult. As far as this point is concerned, previously reported $Z(f,T)$ results in $La_{0.6}Y_{0.1}Ca_{0.3}MnO_3$ and $La_{0.3}Pr_{0.4}Ca_{0.3}MnO_3$ compounds also revealed two components in the frequency domain, which were related to the coexistence of clusters of phases with different transport and magnetic properties [18, 19]. In $La_{0.6}Y_{0.1}Ca_{0.3}MnO_3$ compounds, these clusters were found to coexist in a large temperature range, including a temperature range far above T_C [4]. In addition to this, the LF component was associated with relaxation processes of charge carriers at the interfaces of the AFI/PM and FM clusters, or even to domain walls belonging to clusters of the FM phase [18, 19].

In order to shed some light on the nature of the two observed relaxations in the $Z(f,T,H)$ diagrams the so-called brick layer (BL) model has been applied to the experimental results [26]. By assuming that the LF component is related to a relaxation process at interfaces of the material and using the BL model, the thickness δ_{LF}, and the specific resistivity of a typical interface layer ρ_{LF} can be estimated. The basic assumption of the model is that the microstructure of a given polycrystalline specimen can be represented by a discrete arrangement of cubic regions (representing physical grains with average size d_g) separated by flat boundaries, with both regions having the same dielectric constant [26]. Accordingly, the effective thickness of the interface δ_{LF} can be calculated from $\delta_{LF} = d_g\, C_{HF}/C_{LF}$, and the specific resistivity of the interface is $\rho_{LF} = (R_{LF}C_{LF}/R_{HF}C_{HF})\ r_{HF}$ [27]. The calculated δ_{LF} values ~0.030 μm and ~0.035 μm for $H = 0$ and 1 T, respectively, are smaller than the average grain size determined by SEM analysis (~0.5 μm), and indicate that the application of a magnetic field results in an increase of the effective thickness of the interface. On the other hand, the calculated ρ_{LF} is one order of magnitude higher than r_{HF} and exhibits the largest MR(%) effect close to T_{MI}, as shown in Figs. 3 and 4. Thus, by modeling our polycrystalline samples via the BL model, the application of magnetic fields close to T_{MI} results in an increase of the thickness of the interface layer. Such an increase of the thickness of the interface layer is accompanied by a significant decrease of the specific resistivity ρ_{LF}, suggesting that the assumed interfacial layer between grains (or clusters) exhibits features of the FM metallic phase. Based on these estimates, one is able to infer that increasing applied magnetic field results in an increase of the volume fraction (VF) of the FM phase within the material. Such an increase of VF of the FM phases is of interest and consistent with the phase-separation scenario for manganites in which the application of a magnetic field favors the FM and metallic phase mostly close to T_{MI} [28].

The discussion made above is suitable for the understanding of the general physical properties of the disordered manganite $La_{0.6}Y_{0.1}Ca_{0.3}MnO_3$ studied here. This compound is believed to be comprised of clusters of both FM and AFI/PM phases which coexist in a wide temperature range and have their sizes and VF controlled by changes in both T and H [4, 29]. Within this context, it is more likely that both HF and LF components of the impedance diagrams contain convoluted contributions arising from the different transport processes within grains (or clusters) and through the different interfaces, respectively. However, it is important to point out that the experimental results and the application of the BL model suggest that the LF relaxation process encloses the contribution arising from the FM phase/interfaces.

In order to further investigate the role of the applied H on the electrical properties of this manganite, the impedance data was transformed into dielectric permittivity using the relation: $\varepsilon = 1/(Z\, j\, \omega\, C_0) = \varepsilon' + j\, \varepsilon''$, where j is the imaginary unit, $\omega = 2\pi f$ is the angular frequency, and C_0 is the capacitance of the free space. The permittivity is considered as an important parameter for models of phase separation involving the segregation of doped charge carriers on a mesoscopic scale [30, 31]. Although relatively scarce, an increasingly number of studies regarding the dielectric behavior of manganites has been recently reported, mostly concerning the charge-ordered (Ca, Sr)-doped $PrMnO_3$ systems [32–34]. The obtained values of the real part of the dielectric permittivity (ε') as a function of temperature and frequency for both $H = 0$ and 1 T are displayed in Fig. 5. Values of ε', roughly ranging from 20 to 100, are within the usually reported range for perovskites and large, or sometimes referred to as colossal values of ε' ($>10^3$), have not been observed in the present investigation [30–35]. Such a feature adds further evidence to the intrinsic nature of the measured low frequency (LF) relaxation process (see Fig. 2) since colossal ε' values have been frequently

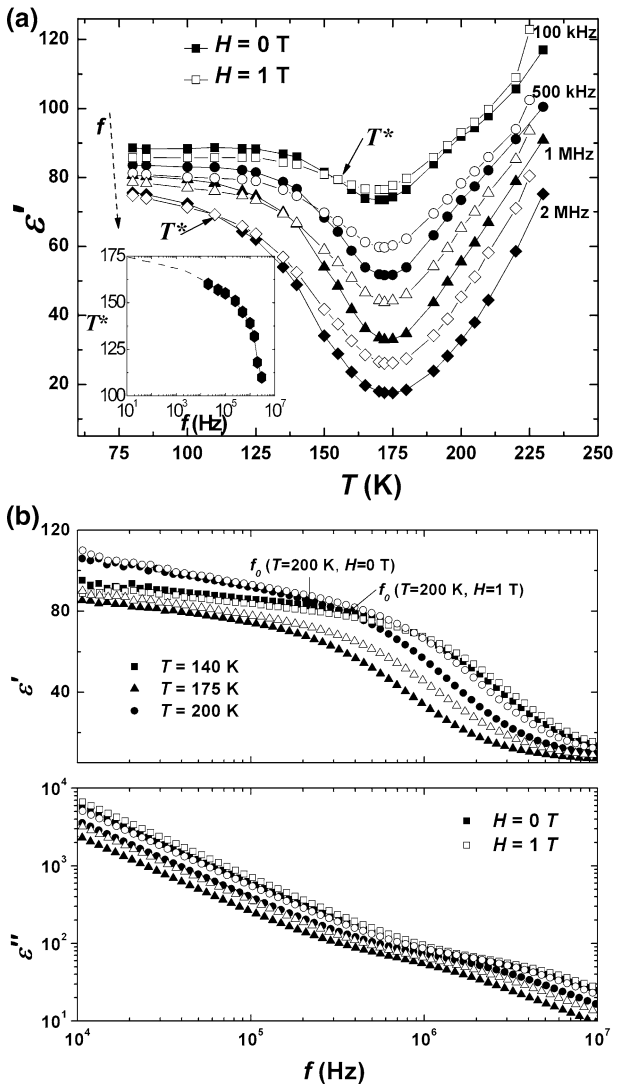

Fig. 5 (**a**) Temperature dependence of the real part of the electrical permittivity ε' measured in both $H = 0$ and 1 T for selected frequencies. The inset shows the T^* dependence on the frequency. (**b**) Frequency dependence of the real and imaginary parts of the electrical permittivity ε measured in both $H = 0$ and 1 T for $T = 140$, 175, and 200 K

ascribed to Schottky effects at the electrode contact [35], except for the so-called multiferroic materials [36].

Let us first consider the temperature dependence of ε' displayed in Fig. 5(a) for some selected frequencies. Two important features are observed in Fig. 5(a): (i) an anomaly of the ε', seen as a minimum close to T_{MI}, that shifts to slightly higher temperatures with increasing f, in agreement with the $Z(f,T,H)$ data; and (ii) increasing f decreases ε', resulting in a more pronounced minimum at $T \sim T_{MI}$. The data indicate values of $\varepsilon' \sim 80$ and that these values are essentially independent of temperature, applied magnetic field, and frequency at $T \ll T_{MI}$. Such a constant value of ε' at low T follows the same trend as $\rho(T \ll T_{MI})$ data, and is probably associated with the small VF variation of the FM metallic phase once the percolative transition has been attained at much higher temperature $T \sim T_{MI}$. On the other hand, close to the MI transition, the pronounced variation of ε' reflects the coexistence of the different phases. Approaching the MI transition from high temperatures, the large increase of $\rho(T)$ evidences that the localized charge carriers of the insulating clusters have a larger VF than the metallic ones (delocalized charge carriers). In fact, FM and AFI fluctuations are believed to occur close to the T_{MI}, and the AFI phase dominates the charge transport acting as traps of the e_g mobile holes as the VF of the FM phase is below the percolation threshold. Such an effect is enhanced by the partial substitution of Y for La in $La_{0.7}Ca_{0.3}MnO_3$ compounds, which weakens the double-exchange mechanisms, and favors the antiferromagnetic super-exchange interaction. As the ac electric field probes the hopping of holes between clusters and also the charge carrier concentration discontinuity across the domain walls, the decrease of ε' close to MI is probably related to the decreased number of mobile charge carriers across the metal-insulator transition. Setting $H = 1$ T results in an increase of the VF fraction of the FM clusters (mobile holes) and a less pronounced decrease of ε' close to T_{MI}, a behavior that is more evident at higher frequencies.

The discussed features are reflected in the data shown in Fig. 5(b), where the frequency dependence of ε for some selected temperatures is displayed. It is possible to identify the ε' relaxation as a step decrease for frequencies above the relaxation frequency $f_0 = (2\pi RC)^{-1}$, as already defined. Values of f_0 were found in the range 10^5–10^6 Hz. The log plot of the imaginary part ε'' exhibits a linear decrease with increasing frequency up to f_0, where a small deviation is coincident with the ε' relaxation occurring in this frequency range. However, no clear dissipation peak was observed in the frequency range investigated, and no significant dependence on the applied magnetic field was observed in the ε'' data. In the frequency range displayed in Fig. 5(b), the relaxation ε' is associated with the low frequency (LF) component of the impedance diagrams, and both relax at the same f_0. For $f < f_0$, ε' exhibits a weak frequency-dependence in the metallic state ($T < T_{MI}$). On the other hand, increasing T above the MI transition results in a more pronounced decrease in ε' with increasing f. The applied magnetic field results in interesting effects on the dielectric properties of the $La_{0.6}Y_{0.1}Ca_{0.3}MnO_3$. At a fixed frequency (Fig. 5(a)), the application of a magnetic filed of $H = 1$ T products a slight decrease of ε' at low temperatures ($T < T_{MI}$). However, we have also evaluated a crossover temperature $T^* < T_{MI}$, a temperature in which ε' (T, $H \neq 0$) assumes values close to ε' (T, $H = 0$) for all the frequencies investigated. Such an increase of ε' above T^* with applied H is more discernible at high frequency and close to the MI transition. It is interesting to note that T^*

increases with decreasing frequency, and apparently moves towards T_{MI} approaching the dc limit (see inset of Fig. 5(a)). Such a behavior is certainly related to the coexistence of FM and PM phases below T_{MI}, in accordance with Mössbauer spectroscopy data for the $La_{0.6}Y_{0.1}Ca_{0.3}Mn^{57}_{0.99}Fe_{0.01}O_3$ compound that indicated a severe competition between PM and ordered phases down to $T \sim 20$ K [29]. The data displayed in Fig. 5(b) also reveals that the application of a magnetic field $H = 1$ T results in a small decrease of ε' for $f < f_0$, and an increase for frequencies above the relaxation, provided that the temperature is maintained constant and below T_{MI}. However, the macroscopic behavior of ε' differs for $T \geq T_{MI}$, and an increase of ε' is observed in the whole frequency range with $H = 1$ T. The ε' dependence on the magnetic field is more pronounced close to T_{MI}, similarly to the CMR effect (Fig. 1), and more evident at frequencies close to f_0. In fact, this observation reflects the shift of f_0 to higher values upon the application of a magnetic field (see Fig. 5(b)). Such an increase of f_0 with H indicates an acceleration of the relaxational dynamics by the application of a magnetic field. In addition, the increase of ε' is in agreement with the decrease of the activation energy for hopping conductivity of the insulating state with applied H [32].

Conclusions

The ac and dc transport properties of single-phase $La_{0.6}Y_{0.1}Ca_{0.3}MnO_3$ specimens prepared by the sol–gel technique were studied. The compound was found to exhibit a metal-insulator transition at essentially the same temperature of the ferromagnetic transition (~175 K). The ac and dc magnetoresistance effects were found to be maximum at temperatures close to the metal-insulator transition. In addition, impedance spectroscopy measurements under applied magnetic field revealed that an interfacial contribution accounts for the magnetoresistance observed at low fields, supporting the scenario where an appreciable intergranular magnetoresistance is expected at low applied magnetic fields. The magnetodielectric properties of the phase separated manganite displaying a metal-insulator transition have been also investigated. The experimental results give further support to the phase separation scenario, as the dielectric permittivity of both the ferromagnetic-metallic and the paramagnetic-insulating phases was found to exhibit different dependence on both the frequency and the applied magnetic field.

Acknowledgments This work was partially supported by the Brazilian agencies FAPESP (01/04231-0, 02/01856-1, and 05/53241-9) and CNPq (303272/2004-0, 306496/88-7, 300934/94-7, and 301661/2004-9).

References

1. Tokura Y (ed) (2000) Colossal magnetoresistance oxides. Gordon & Breach, New York
2. Jin S, Tiefel H, McCornack M, Fastnacht RA, Ramesh R,Chen LH (1994) Science 264:413
3. Burgy J, Moreo A, Dagotto E (2004) Phys Rev Lett 92:097202
4. Souza JA, Jardim RF (2005) Phys Rev B 71:054404
5. Dagoto E, Hotta T, Moreo A (2001) Phys Rep 344:1
6. Uehara M, Mori S, Chen CH, Cheong SW (1999) Nature 399:560
7. Hwang HY, Cheong S-W, Ong NP, Batlogg B (1996) Phys Rev Lett 77:2041
8. Fu YL (2000) Appl Phys Lett 77:118
9. Moreo A, Yunoki S, Dagotto E (1999) Science 283:2034
10. Schiffer PE, Ramirez AP, Bao W, Cheong SW (1995) Phys Rev Lett 75:3336
11. Fontcuberta J, Martnez B, Seffar A, Piñol S, Garcia-Muñoz JL, Obradors X (1996) Phys Rev Lett 76:1122
12. Maignan A, Sindaresan A, Varadaju UV, Raveau B (1998) J Magn Magn Mater 184:83
13. Shah WH, Hasanain SK (2002) J Magn Magn Mater 246:199
14. Hu J, Qin H, Niu H, Zhu L, Chen J, Xiao W, Pei Y (2003) J Magn Magn Mater 261:105
15. Glaser A, Ziese M (2002) Phys Rev B 66:094422
16. Castro GMB, Rodrigues AR, Machado FLA, de Araujo AEP, Jardim RF, Nigam AK (2004) J Alloy Compd 369:108
17. Carneiro AS, Fonseca FC, Jardim RF, Kimura T (2003) J Appl Phys 93:8074
18. Souza JA, Jardim RF, Muccillo R, Muccillo ENS, Torikachvili MS, Neumeier JJ (2001) J Appl Phys 89:6636
19. Fonseca FC, Souza JA, Jardim RF, Muccillo R, Muccillo ENS, Gouvêa D, Jung MH, Lacerda AH (2003) Phys Status Solidi A 199:255
20. Fonseca FC, Souza JA, Jardim RF, Muccillo R, Muccillo ENS, Gouvea D, Jung MH, Lacerda AH (2004) J Eur Ceram Soc 24:1271
21. Bauerle J (1969) J Phys Chem Solids 30:2657
22. Fonseca FC, Muccillo R (2002) Solid State Ionics 149:309
23. Escote MT, da Silva AM, Matos JR, Jardim RF (2000) J Solid State Chem 151:298
24. Wang YX, Du Y, Qin RW, Han B, Du J, Lin JH (2001) J Solid State Chem 156:237
25. Fletcher JG, West AR, Irvine JTS (1995) J Electrochem Soc 142:2650
26. van Dijk T, Burggraaf AJ (1981) Phys Status Solid A 63:229
27. Guo X, Sigle W, Fleig J, Maier J (2002) Solid States Ionics 154–155:555
28. Moreo A, Yunoki S, Dagotto E (1999) Science 283:2034
29. Goya GF, Souza JA, Jardim RF (2002) J Appl Phys 91:7932
30. Cohn JL, Peterca M, Neumeier JJ (2004) Phys Rev B 70:214433
31. Wang CC, Cui YM, Xie GL, Chen CP, Zhang LW (2005) Phys Rev B 72:064513
32. Freitas RS, Mitchell JF, Schiffer P (2005) Phys Rev B 72:144429
33. Biškup N, de Andrés A, Martinez JL (2005) Phys Rev B 72:024115
34. Pimenov A, Biberacher M, Ivannikov D, Loidl A, Mukhin AA, Goncharov YuG, Balbashov AM (2006) Phys Rev B 73:220407
35. See, for example, Lunkenheimer P, Fichtl R, Ebbinghaus SG, Loidl A (2004) Phys Rev B 70:17210; Lunkenheimer P, Bobnar V, Pronin AV, Ritus AI, Volvok AA, Loidl A (2002) Phys. Rev. B 66:052105
36. Kimura T, Goto T, Shintani H, Ishizaka K, Arima T, Tokura Y (2003) Nature 426:55